Journal of Biomechanics 90 (2019) 92–102

Contents lists available at ScienceDirect

Journal of Biomechanics

journal homepage: www.elsevier.com/locate/jbiomech
www.JBiomech.com

# Validation of subject-specific musculoskeletal models using the anatomical reachable 3-D workspace

Miguel Nobre Castro *, John Rasmussen, Shaoping Bai, Michael Skipper Andersen

*Department of Materials and Production, Aalborg University, DK-9220 Aalborg East, Denmark*

ARTICLE INFO

*Article history:*
Accepted 26 April 2019

*Keywords:*
Musculoskeletal modelling
Subject-specific model validation
Reachable 3-D workspace
Strength measurements
Upper extremity biomechanics

ABSTRACT

A novel metric for the validation of musculoskeletal models is proposed, the reachable 3-D workspace (RWS). This new metric was used to compare a generic model scaled in a standard manner to a more subject-specific model. An experimental protocol for assessing the RWS was performed by ten participants for four distinct hand-payload cases. In addition, isometric individual strength measurements were collected for 12 different directions. The strength of subject-specific musculoskeletal models was then computed using the following assumptions: (1) standard routines including the length-mass-fat (LMF) scaling law; (2) the isometric strengths of the muscle elements were optimized to the individual strength measurements using joint strength factors (JSF). The RWS of each participant was subsequently estimated from each of the scaling approaches, LMF and JSF, for the four load cases. The experimental RWS showed that the volume and shape decreased with increasing hand-payload for every participant. The lateral and frontal far-from-torso aspects of the RWS were reduced the most. These trends were reproduced by both strength scaling approaches, but the LMF-scaled models were not able to track the overall RWS volume decrease with increasing payload, since they proved to be weaker than the participants. On the other hand, the optimised JSF subject-specific models performed better on the prediction of the RWS for all payload cases across participants. The RWS can potentially be further used as a subject-specific musculoskeletal model validation, enabling quantification of the volume and shape differences between experimentally and model-predicted RWSs.

## 1. Introduction

Musculoskeletal models are useful for estimating biomechanical variables such as joint reactions and muscle forces. These models can help understand the underlying factors of musculoskeletal disorders/injuries, improve treatment and rehabilitation (Fregly et al., 2012; Sartori et al., 2016), and predict surgery/intervention outcomes (Fischer et al., 2018; Quental et al., 2013). Other applications include product design in ergonomics (Pontonnier et al., 2014; Wu et al., 2009) and sports research/development (Lee et al., 2017; Rasmussen et al., 2012).

Commonly, these models include muscle-tendon units. The Hill-type model comprises a contractile element along with parallel and serial-elastic elements (Zajac, 1989). Contraction dynamics are formulated by force-length-velocity relationships that depend on various parameters: isometric strength; optimal fibre length; pennation angle; absolute contraction velocity; and tendon slack length. Predictions previously attempted by these models were sensitive to these parameters and it is, therefore, important to identify them for the subjects analysed (Ackland et al., 2012; Carbone et al., 2016; De Groote et al., 2010; Redl et al., 2007). To this end, Heinen et al. (2016) reported few methods to determine these parameters, involving extensive strength measurements, sometimes requiring expensive equipment such as isokinetic dynamometers (Garner and Pandy, 2003; Lloyd and Besier, 2003) or time-consuming segmentation of medical images (Bolsterlee et al., 2015; Valente et al., 2014).

Given the uncertainty of many of their parameters, validation of musculoskeletal models is crucial. Kinetically speaking, ground reaction forces (Fluit et al., 2014), implant reaction forces (Marra et al., 2015) and tendon forces (Fleming and Beynnon, 2004) have been used as validation metrics. The latter two of these validation methods are invasive and therefore not practical for common use.

The reachable 3-D workspace (RWS) describes the region or volume that a point in the hand/wrist can reach with at least one orientation (Klopčar et al., 2007). It provides an insight into motor function for both healthy and disabled individuals (Matthew

---

* Corresponding author at: Department of Materials and Production – Aalborg University, Fibigerstraede 16, DK-9220 Aalborg East, Denmark.

*E-mail addresses:* mnc@mp.aau.dk (M.N. Castro), jr@mp.aau.dk (J. Rasmussen), shb@mp.aau.dk (S. Bai), msa@mp.aau.dk (M.S. Andersen).

https://doi.org/10.1016/j.jbiomech.2019.04.037
0021-9290/© 2019 Elsevier Ltd. All rights reserved.

et al., 2015). Given its kinetic nature (Castro et al., 2019; Han et al., 2015), it can potentially be simulated on musculoskeletal models to evaluate performance and strength. Moreover, according to the distinctions of Lund et al. (2012), the RWS can be a direct validation measure since it can be recorded in-vivo and musculoskeletal models set up to produce directly comparable outputs.

To the best of our knowledge, no attempt has been made to use the RWS as a validation metric. Hence, the aims of this study were: (1) to evaluate a low-cost setup for subject-specific model calibration, (2) to test the use of the RWS as a new validation metric, (3) to compare default scaled against strength scaled models.

## 2. Materials and methods

### 2.1. Experimental procedures

Ten males (age 30.0 ± 8.0; body mass 78.9 ± 10.8 kg; height 1.80 ± 0.06 m; upper extremity length 0.644 ± 0.027 m – details in the Supplementary Material) volunteered for this study with the following inclusion criteria: healthy with no abnormalities in the upper extremity bone structure or missing limbs, and absence of any type of injury at the time of data collection. Written informed consent was obtained and the ethical guidelines of The North Denmark Region Committee on Health Research Ethics were followed. The experiment comprised two assessments (1) the kinematics of the RWS for four different hand payload cases and (2) the kinematics and kinetics of the maximum force generation capability in a given direction.

A 5-minute warm-up was given to the participants, consisting of random upper extremity motion. A wrist-stabilizing brace (Mueller® Sports Medicine Inc, Wisconsin, USA) was worn to prevent wrist joint motions. An eight-camera setup (Opus, Qualisys AB, Gothenburg, Sweden) was used to collect the trajectories of 19 reflective markers placed on the skin through palpation of specific bony landmarks (Castro et al., 2019).

#### 2.1.1. Kinematic assessment of the reachable 3-D workspace

The assessment of the upper extremity kinematics followed the RWS protocol proposed in our previous study (Castro et al., 2019). Each test subject was guided by an assistant performing a mirrored version of the movement protocol for each task to capture the RWS boundaries. The protocol was repeated for four different hand payload cases, performed in four distinct days to avoid fatigue (20 trials per subject, five per day). The first "no-payload" case corresponded to the active RWS while the other three payload cases were selected to result in a gradual RWS volume decrease by increase of the dumbbell mass. A shoulder abduction task was performed three times at a slow pace with different payloads between 8 and 12 kg, was used to individually select suitable dumbbell masses. The one-repetition maximum abduction angle closest to 90° was defined as the threshold payload, i.e. the third load case. The other load values were selected if they reflected abduction angle differences of 30° below (60°) or above (120°) that 90° threshold, otherwise the respective payload was decreased or increased by 2 kg, respectively. Fatigue propagation was avoided by limiting the number of these attempts to three. All payload masses are provided in the Supplementary Material.

#### 2.1.2. Kinetic assessment of the maximum force generation capability

The maximum force generation capability, $F_{max}$, was measured for a set of three different postures close to that corresponding to the maximal torque generation angle for each of the 12 directions shown in Fig. 1. These directions corresponded to canonical anatomical movements. The three postures were approximately separated by angular differences up to 30°: as an example, elbow flexion was measured for the angles of 60°, 90° and 120°. The participants pulled against a force sensor (Universal Digital Dynamometer, Tiedemann & Betz GmbH & Co, Garmisch-Partenkirchen, Germany) strapped to a metallic structure while seated and instructed to lean back on a chair fixed to the same metallic structure without moving the trunk. Three extra markers were placed on the sensor and on the brace to identify this external force vector and application point in space. Thirty-six isometric maximum voluntary contraction (MVC) measurements were performed per participant. Fatigue was avoided by performing this assessment on the same day as the "no-payload" case, by taking a resting period of one minute between each measurement, and by taking a 2–5 min break between different directions. The directions were selected such that two consecutive measurements targeted different muscle groups and such order varied across subjects. All participants were vocally encouraged to attain a MVC.

### 2.2. Computational methods

#### 2.2.1. Musculoskeletal modelling

Musculoskeletal models were built in the AnyBody Modeling System (AMS) v.6.0.5 (AnyBody Technology A/S, Aalborg, Denmark) from the 'Standing Model' (AMMRv.1.6.3), which is based on the lumbar spine data from the work of de Zee et al. (2007) and on shoulder, upper- and lower-arm data from the Delft Shoulder Group (Van der Helm et al., 1992; Veeger et al., 1997; 1991). The model comprised the right upper extremity and a rigid trunk (thorax, lumbar spine and pelvis) segment, which allowed eight-degrees-of-freedom (DOF): a sternoclavicular (three-DOF), glenohumeral (three-DOF), and elbow and forearm (two-DOF) joints. Wrist joint motion was excluded, and the scapula was constrained to slide on the rib cage. The model was actuated by 140 Hill-type muscle elements. Their tendon slack length was adjusted using the One-step Calibration method, which defines these according to joint positions corresponding to optimal muscle fibre lengths (Heinen et al., 2016). All inverse dynamic analyses followed the Newton-Euler formulation described by Damsgaard et al. (2006).

*2.2.1.1. Geometric scaling, motion reconstruction and boundary conditions.* A kinematic-only copy of the musculoskeletal model was primarily defined without muscles. This 'Mocap Model' was used to geometrically scale the 'Standing Model'. A length-mass specific linear scaling law that relates each segment length with its mass was applied (Rasmussen et al., 2005). Subsequently, the maker coordinate data of a standing static trial were used to identify the location of markers not placed on bony landmarks using the method of Andersen et al. (2010) (see the marker protocol in the Supplementary Material). Simultaneously, this method adjusted the dimensions of all segments including the hand breadth but excluding the pelvis width and the head height. The resultant measures were input to the 'Standing Model'.

The joint angles recorded during the kinematic and kinetic assessments were retrieved using the 'Mocap Model' by driving it with the optimised marker trajectories as formulated by Andersen et al. (2009). These joint angles were later used as inputs for the 'Standing Model'.

The boundary conditions for the 'Standing Model' simulations were set as following: (1) the rigid trunk segment was grounded, (2) the dumbbells used in the kinematic assessment were modelled as an extra spherical segment attached to the palm of the hand, (3) the dynamometer external force vector was given by two markers placed on the sensor (Fig. 2) and its application point by the projection of a third marker placed on the brace onto the longitudinal axis of the respective segment (humerus, ulna or hand).

**Fig. 1.** The 12 directions selected for strength measurements on which the participant pulled against a force sensor (dynamometer): (1) shoulder elevation and depression, (2) shoulder flexion and extension, (3) shoulder abduction and adduction, (4) shoulder external and internal rotations, (5) elbow flexion and extension, (6) push and pull. Three measurements were taken per direction for different joint angles. All participants were vocally encouraged to maximize their voluntary muscle contraction.

### *2.2.1.2. Strength scaling.*

*2.2.1.2.1. Length-mass-fat scaled model.* The ‘Standing Model’ was initially strength-scaled using a length-mass-fat (LMF) scaling law that adjusted the muscle’s isometric strength through regression studies (Frankenfield et al., 2001) that account for both anthropometrics and fat percentage of the body segments (Rasmussen et al., 2005).

*2.2.1.2.2. Joint-strength-factors scaled model.* The subject-specificity of the above mentioned LMF models was enhanced using the participants’ strength measurements. Accordingly, the muscle elements were assigned to one or more of 15 groups (Table 1), which enabled definition of 16 joint-strength-factors (JSFs) capable of improving their isometric strength. Such grouping followed the muscles action (Moore and Agur, 2007) and their

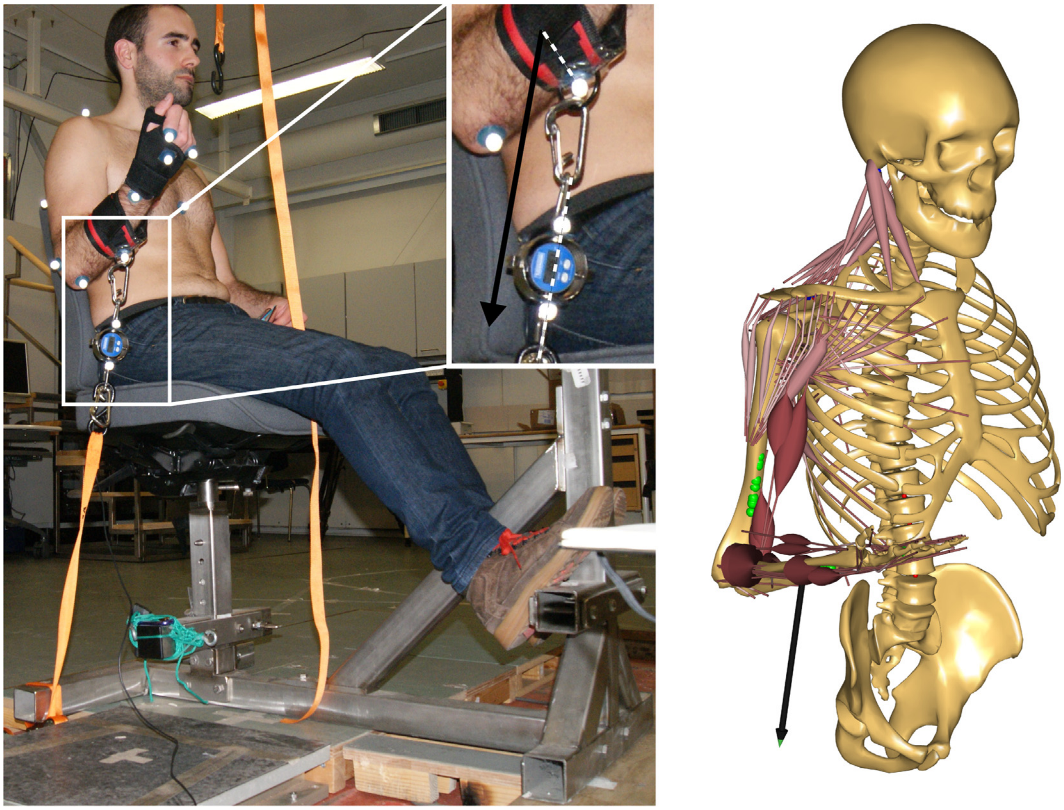

**Fig. 2.** (Left) The strength measurement setup with the force sensor positioned for a measurement about the elbow flexion direction; (Right) The respective static posture was collected and modelled in AMS to perform an inverse dynamic analysis. The direction of the external force measured by the force sensor was given by the two markers attached to the sensor. A third marker was projected in the longitudinal axes of the ulna bone (green marker) on the model) to serve as the force application point. (For interpretation of the references to colour in this figure legend, the reader is referred to the web version of this article.)

lever-arm contribution to each canonical joint movement in the model. Please note that many muscles in the forearm, such as the brachioradialis, share both pronation and supination JSFs as their contribution depends on the forearm posture.

An overall maximal muscle activation (MMACT), i.e. force divided by instantaneous strength, is obtained after performing an inverse dynamic analysis. By using a min/max muscle recruitment criterion (Rasmussen et al., 2001), an activation function $a_k(\mathbf{s}^{(D)})$ depending on a n-dimensional ($n^{(D)}$) vector $\mathbf{s}^{(D)}$ containing all JSFs was defined as:

$$a(\mathbf{s}^{(D)}) = \min_{\mathbf{f}\in\mathbb{R}} \max\left(\frac{f_i^{(M)}}{N_i s_1 \prod_j^{d_i} s'_{ij}}\right), \quad i = 1,\cdots,n^{(M)}; \quad d_i < n^{(D)} \tag{2}$$

*subject to*

$$\mathbf{Cf}=\mathbf{r}$$

$$f_i^{(M)} \geq 0, i = 1,\cdots,n^{(M)}$$

where with regard to the i^th^ muscle, $f_i^{(M)}$ is the force generated, $N_i$ is the instantaneous strength, $s_1$ is the global JSF and first element of $\mathbf{s}^{(D)}$, and $s'_{ij}$ is the j^th^ entry of all $d_i$ JSFs that pre-multiply the i^th^ muscle. As constraints, $\mathbf{C}=\left[\mathbf{C}^{(M)} \; \mathbf{C}^{(R)}\right]$ is a matrix of coefficients depending on the current global position of the model segments, $\mathbf{f}=\left[\mathbf{f}^{(M)T}\mathbf{f}^{(R)T}\right]^T$ is a vector of unknown muscle (M) and reaction forces (R), and $\mathbf{r}$ is a right-hand side vector composed of external and inertial forces.

Since a MVC implies that at least one synergist muscle is fully activated, an optimisation problem was formulated in a least-squares approach to fit the models to the strength measurements. The optimum set of JSFs was found by minimizing the squared difference between the MMACT and a full activation state:

$$\min_{\mathbf{s}\in\mathbb{R}} \sum_{k=1}^{n^{(P)}} \left(a_k(\mathbf{s}^{(D)}) - 1\right)^2 \tag{3}$$

*subject to*

$$b_{\text{lower}} \leq s_l \leq b_{\text{upper}}, \qquad l = 1,\cdots,n^{(D)}; \qquad b_{\text{lower}}, b_{\text{upper}} \in \mathbb{R}_0^+$$

$$0 \leq s_1 \prod_j^{d_i} s'_{ij} \leq 3, \qquad i = 1,\cdots,n^{(M)}$$

where $a_k$ is the inverse dynamic analysis activation outcome of the k^th^ strength measurement, $s_l$ is an entry of the vector $\mathbf{s}^{(D)}$ that is bounded between the current search space's lower and upper values $b$, and lastly $s_1 \prod_j^{d_i} s'_{ij}$ is the JSF product of the i^th^ muscle. The initial search space boundaries $b$ should be set manually in the vicinity of the solution where all JSFs are equal to one, as this would correspond to the equivalent LMF model. According to the findings by Garner and Pandy (2003) reporting that isometric strength can scale two to three times in models based on the Delft Shoulder Groups studies, each of these JSF products was only allowed to vary between values of 0 and 3.

Accordingly, a two-level optimisation routine was implemented in MATLAB® (MathWorks Inc., Natick, MA USA). First, 36 ($n^{(P)}$) analytical response surfaces (i.e. surrogate models) were created to define the sensitivity of the activation function $a_k(\mathbf{s}^{(D)})$ of each k^th^ strength measurement towards the JSFs. A Box-Behnken experiment design (Box and Behnken, 1960) implies that the minimum set of sample points required to create a 16-D multivariate linear

**Table 1**
General list of muscles covered by each Joint Strength Factors (JSF). Further AMS-specific details can be found in the Supplementary Material.

| Joint Strength Factor | Muscles |
|---|---|
| Global | All muscles |
| SCProtraction | Pectoralis major and minor; Serratus anterior |
| SCRetraction | Trapezius descending, middle and ascending; Rhomboids major and minor |
| SCElevation | Trapezius descending and middle; Levator scapulae; Sternocleidomastoid |
| SCDepression | Pectoralis major and minor; Trapezius ascending; Latissimus dorsi |
| Scapula Stabilization | Trapezius ascending and middle; Levator scapulae; Rhomboids minor and major; Pectoralis minor; Serratus anterior |
| GHFlexion | Deltoid anterior; Pectoralis major; Biceps brachii short and long heads; Coracobrachialis |
| GHExtension | Pectoralis major sternocostal head; Latissimus dorsi; Deltoid posterior; Infraspinatus; Teres minor; Triceps brachii long head |
| GHAbduction | Deltoid middle; Supraspinatus |
| GHAdduction | Pectoralis major; Latissimus dorsi; Teres major; Subscapularis; Coracobrachialis |
| GHExtRot | Deltoid posterior; Infraspinatus; Teres minor |
| GHIntRot | Pectoralis major; Latissimus dorsi; Deltoid anterior; Teres major; Subscapularis |
| EFlexion | Biceps brachii short and long heads; Brachialis; Brachioradialis; Supinator humeral head; Pronator teres; Flexor carpi ulnaris and radialis; Extensor carpi ulnaris and radialis; Flexor digitorum superficialis; Extensor digitorum and digiti minimi; Palmaris longus |
| EExtension | Triceps; Anconeus; Flexor carpi ulnaris and radialis; Extensor carpi ulnaris and radialis; Flexor digitorum superficialis; Extensor digiti minimi; Palmaris longus |
| EPronation | Brachioradialis; Pronator teres; Pronator quadratus; Supinator; Anconeus; Flexor carpi ulnaris and radialis; Extensor carpi ulnaris and radialis; Flexor digitorum superficialis and profundus; Extensor digitorum, indicis and digiti minimi; Extensor pollicis longus; Abductor pollicis longus; Palmaris longus |
| ESupination | Biceps brachii short and long heads; Brachioradialis; Supinator; Pronator teres; Pronator quadratus; Flexor carpi ulnaris and radialis; Extensor carpi ulnaris and radialis; Flexor digitorum superficialis and profundus; Extensor digitorum, indicis and digiti minimi; Extensor pollicis longus; Abductor pollicis longus; Palmaris longus |

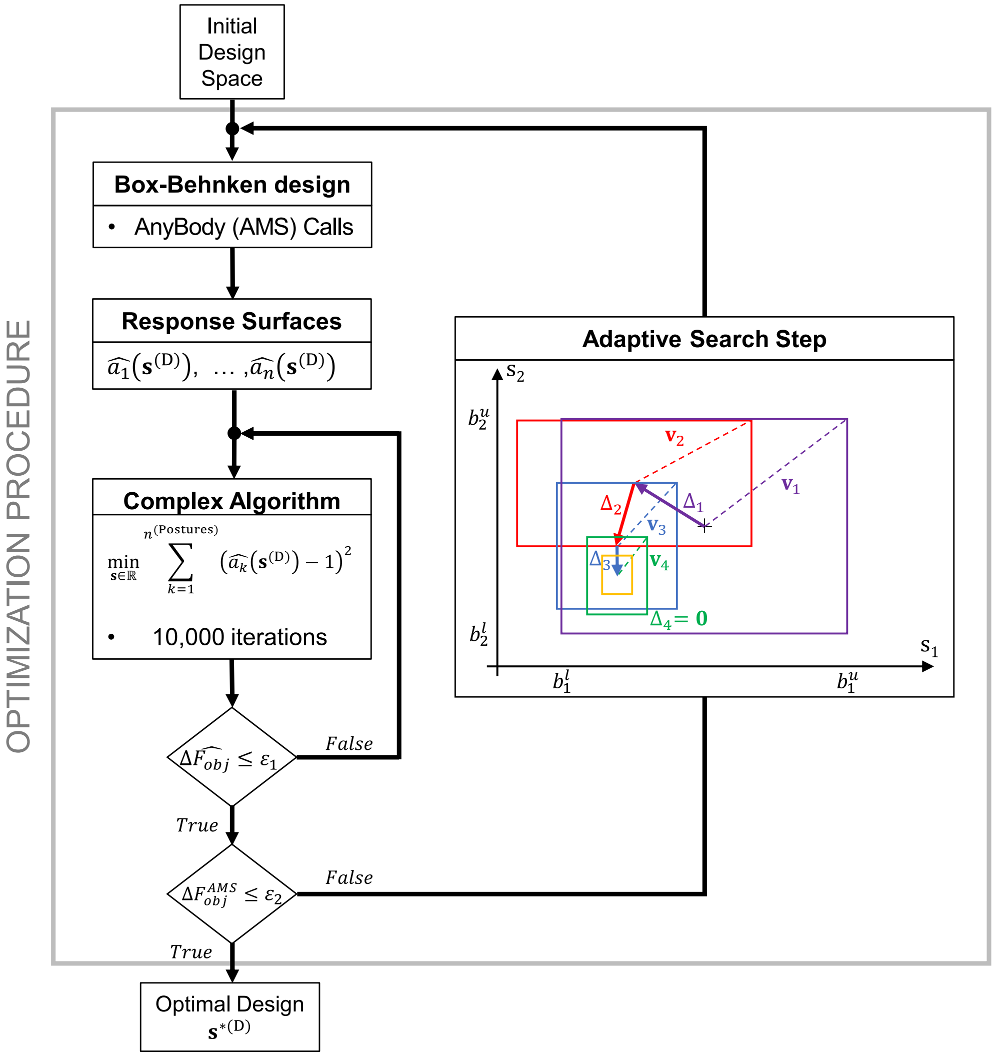

**Fig. 3.** Schematic of the optimization procedure used to obtain the JSF set. The routine is composed of two-loops and uses sequential response surfaces, i.e. surrogate models, to speed-up the Complex Method algorithm (Box, 1965). The outer-loop involves an adaptive search step to allow the adjustment of the design space after each iteration.

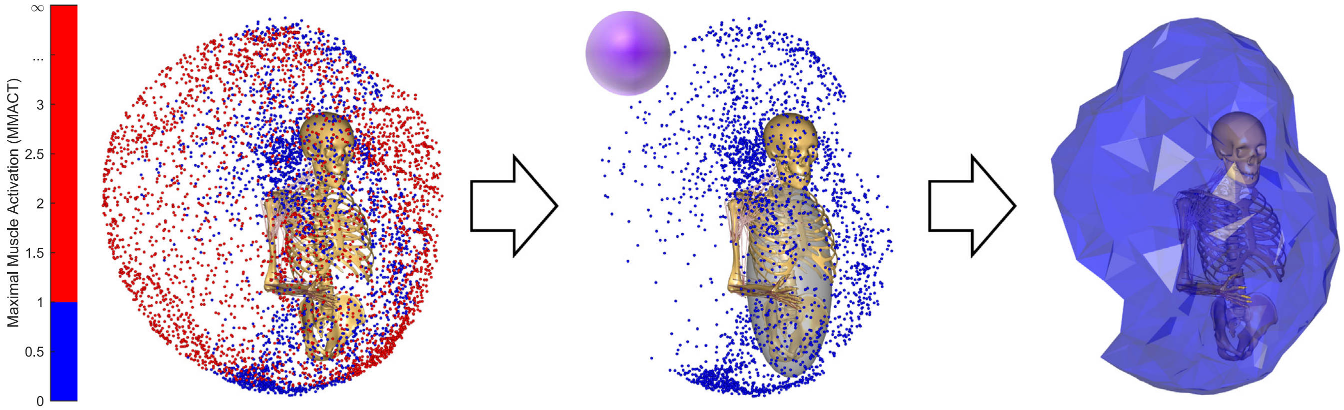

**Fig. 4.** The reconstruction of the RWS for musculoskeletal model validation. In the point cloud resultant from all inverse dynamic analyses for all experimental/mocap postures, blue points are said to be "reachable" if MMACT ≤ 1 while the red ones correspond to "non-reachable" situations, i.e. MMACT > 1. The non-convex envelope shape of the blue "reachable" point cloud is then computed using the alpha-shapes algorithm (Edelsbrunner and Mücke, 1994) by setting the alpha-radius (of the represented sphere) equal to the semi-minor (smallest) axis of the transversal cross-section of the ellipsoid used to model the serratus anterior muscle-tendon units, as described in Castro et al. (2019). (For interpretation of the references to colour in this figure legend, the reader is referred to the web version of this article.)

regression with 2nd-order terms is 396. Thus, 14,256 inverse dynamic analyses were required to evaluate the objective function in Eq. (3). Hence, each regression model was defined according to Eq. (4) (or in matrix form Eqs. (5) and (6)), and solved for its $\theta$ parameters using the orthogonal projection method:

$$a_{kp} \approx \theta_0 + \theta_1 s_{1p} + \cdots + \theta_{\mathrm{D}} s_{\mathrm{D}p} + \theta_{\mathrm{D}+1} {s_{1p}}^2 + \theta_{\mathrm{D}+2} s_{1p} s_{2p} + \cdots \\ + \theta_{2\mathrm{D}+\binom{\mathrm{D}}{2}} {s_{\mathrm{D}p}}^2, \qquad p = 1, \cdots, 396 \tag{4}$$

$$\hat{\boldsymbol{a}}_{\boldsymbol{k}} = \boldsymbol{S\theta} \tag{5}$$

$$\boldsymbol{\theta} = \left(\boldsymbol{S}^T \boldsymbol{S}\right)^{-1} \boldsymbol{S}^T \hat{\boldsymbol{a}}_{\boldsymbol{k}} \tag{6}$$

Secondly, the optimisation routine was implemented using two-levels such that the search space could adapt to the design space as presented in Fig. 3. An inner-loop ran the Complex algorithm (Box, 1965) on Eq. (3) with a population of 100 samples for 10,000 iterations each time, repeatedly, until fulfilment of the stopping criterion that all members in the population had the same objective function within a $\Delta\hat{\boldsymbol{F}}_{\boldsymbol{obj}} = 0.0001$ tolerance. Then, an adaptive outer-loop allowed to move and to zoom in/out the search space window on the full design space to avoid local minima. A parameter $\alpha$ governed this adaptation according to Eq. (7):

$$\mathrm{v}_j^{i+1} = \left(\alpha + (1-\alpha)\frac{{\Delta_j^{\mathrm{i}}}^2}{{\mathrm{v}_j^{\mathrm{i}}}^2}\right)\mathrm{v}_j^i, \qquad j = 1, \cdots, n^{(\mathrm{D})} \tag{7}$$

where the j^th entry of the scaling vector $\mathbf{v}^{\boldsymbol{i}}$, corresponding to the i^th inner-loop run, consists of half of the current $b$ ranges of each design variable $s_l$ (represented by coloured rectangles in Fig. 3); the step vector $\Delta^{\boldsymbol{i}}$ corresponds to the geometric difference between two consecutive inner-loop solutions that converged. The exact $\boldsymbol{F}_{\boldsymbol{obj}}^{\boldsymbol{AMS}}$ was directly assessed using the AMS after each inner-loop convergence and new surrogates were generated every time the

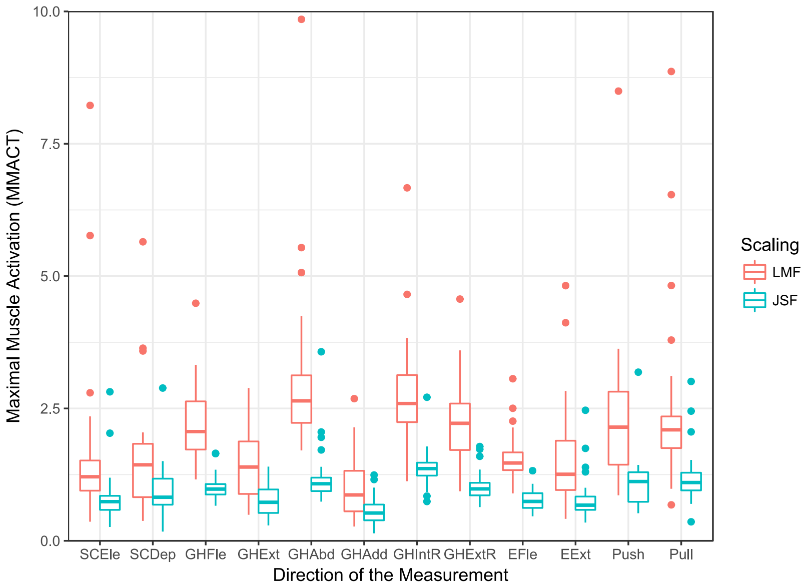

**Fig. 5.** Box plot showing the overall MMACT obtained while simulating the strength measurements for both LMF and JSF models. The three measurements of each participant were grouped according to the direction about which they were performed. The LMF models were overactive while the JSF models were better capable to approximately attain 100% MMACTs.

inner-loop ran. The vector $\Delta$ allowed the search space to scale independently for each design variable. The dimensioning factor $\alpha$ was set to 0.5 and it controlled convergence of the outer-loop of the adaptive optimisation algorithm within an objective function tolerance of $\Delta F_{obj}^{AMS} = 0.01$. The aforementioned bounds $b$ (Eq. (3)) constrained the outer-loop routine on each search step to avoid extrapolation errors outside the surrogate domains. These surrogates enabled evaluating the design space in a wider and fast manner by allowing the implementation of parallel computations. The total computational time was reduced to approximately a week (on a machine operating with 30 CPUs). A model strength-scaled using these JSFs will be designated as a JSF model.

### 2.2.2. Prediction of the reachable workspace

The experimental RWS was reconstructed from the motion capture data points for each load case as presented in Castro et al. (2019), while the musculoskeletal models simulated the RWS using the motion from the no-payload case corresponding to the active RWS. Even though the AMS simulates dynamic models, the joint angles were discretized to individual frames for separate posture analyses (null velocities and accelerations) to agree with the quasi-static nature of all dynamic experimental measurements. Subsequently, the selection of the simulated reachable point cloud followed a simple rule: any point in the Cartesian space is said to be reachable if the MMACT obtained for the respective posture is smaller or equal to one (MMACT $\leq 1$), and not reachable otherwise.

The alpha-shape algorithm (Edelsbrunner and Mücke, 1994) was then applied to retrieve the non-convex shape of the simulated reachable 3-D point cloud. Accordingly, the alpha-radius was set as the semi-minor axis of the transversal cross-section of the ellipsoid used to wrap the serratus anterior muscle elements around the rib cage as described in (Castro et al., 2019) and exemplified in Fig. 4.

The RWS volumes of the meshes corresponding to the experimental ($V_{exp}$), simulated ($V_{sim}$) and respective intersection ($V_{exp} \cap V_{sim}$) and union ($V_{exp} \cup V_{sim}$) were computed in MATLAB and compared. Finally, to avoid potential over-estimation misinterpretations, the corresponding values of Intersection-over-Union (IoU), $(V_{exp} \cap V_{sim})/(V_{exp} \cup V_{sim})$, were reported and the models compared using Wilcoxon Signed Rank tests.

## 3. Results

The evaluation of the optimisation procedure for enhancing the subject-specificity of the model with the addition of strength measurements is presented in Fig. 5. The LMF scaling seemed to produce globally weak models with activations greater than 100% (MMACT $\gg 1$) for the MVCs. The optimised JSF models approximated the strength measurements better, as the overall activations approached 100% (MMACT $\approx 1$).

The JSF products obtained from the optimisation procedure for each muscle element (Fig. 6) showed an increase in all muscles' isometric strengths. In some circumstances, these products reached the upper bound value, i.e. three times the strength values obtained on the LMF models. In some participants, this increase was more evident for the muscles inserting on the scapula, namely supraspinatus, infraspinatus, teres minor and major, subscapularis, posterior and medial deltoids, serratus anterior, pectoralis minor, and lastly also pectoralis major.

The shapes of the reconstructed experimental RWS obtained for one of the participants are presented in Fig. 7. They indicate that the volume of the RWS decreased with increasing hand-payload. This shrinking effect seemed to affect mostly the lateral and frontal

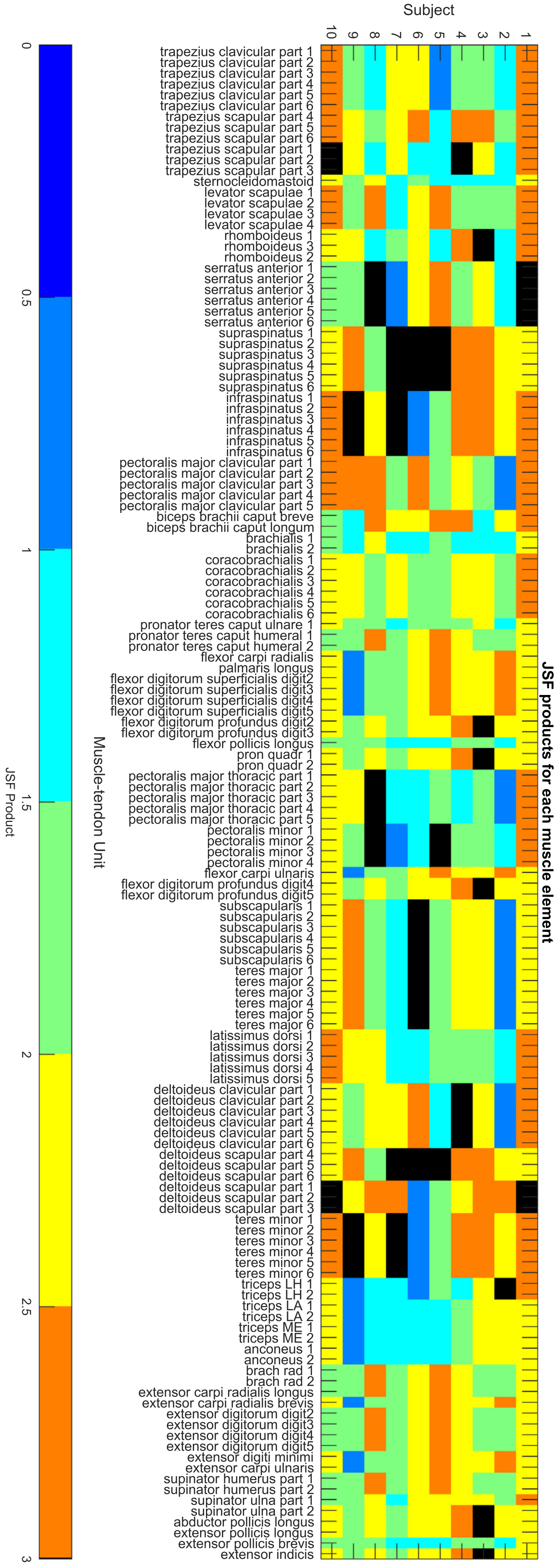

**Fig. 6.** Chart with the pre-multiplying JSFs for each individual muscle-tendon unit. The colour bar represents the scalar grade and the black colour represents values that reached the maximum value of the scale.

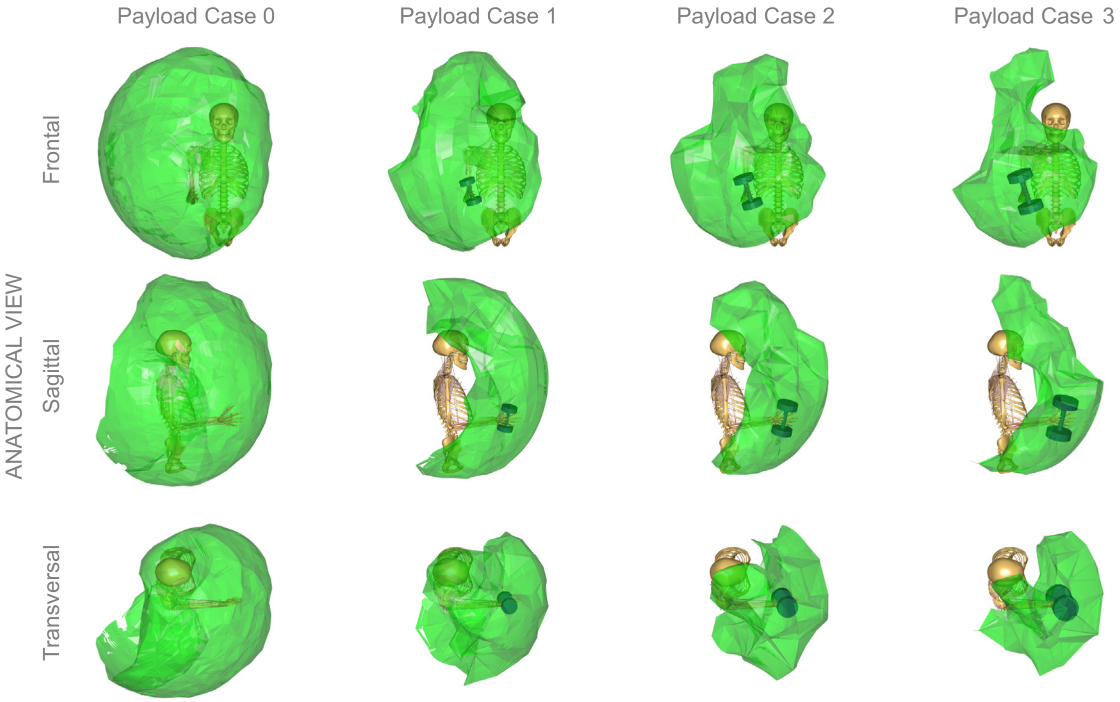

**Fig. 7.** The experimental RWS for one of the participants: no hand payload; first load case, second load case, third load case. The RWS shape shrinks and its volume decreases with increasing hand-payload. The RWS seems to evolve to an hourglass shape.

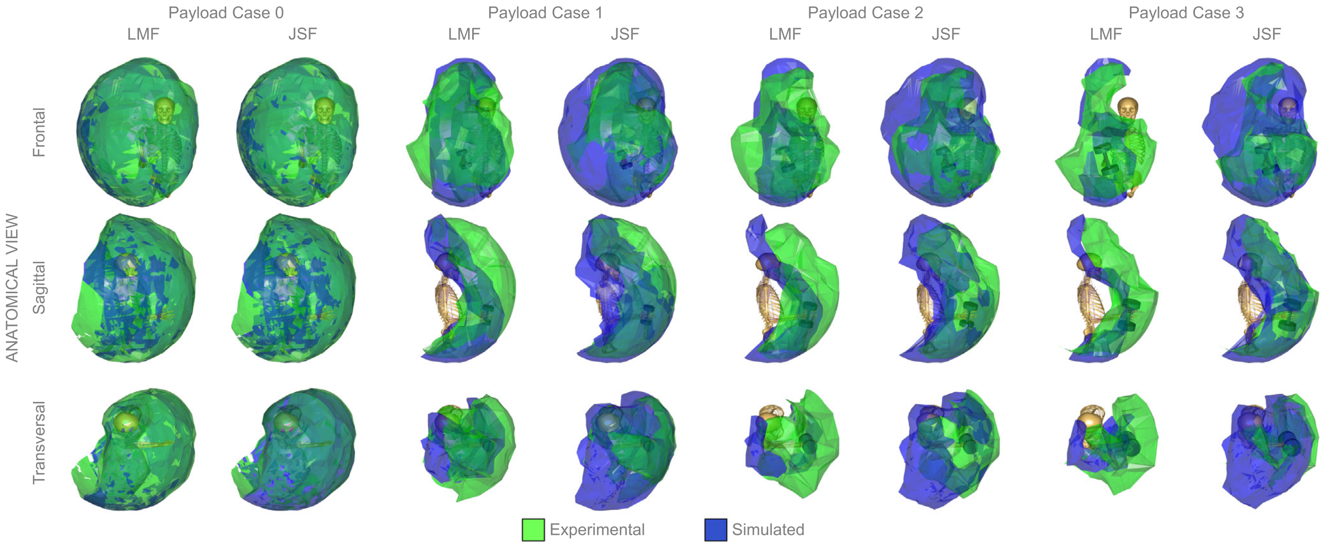

**Fig. 8.** Comparison of the simulated RWS predictions (blue) for both LMF and JSF models against the experimental RWS (green) for the four payload cases in one of the participants. The optimized JSF model seems to better capture the RWS shape for all cases. (For interpretation of the references to colour in this figure legend, the reader is referred to the web version of this article.)

aspects of the RWS. Larger volume and shape differences were detected for the RWS predictions for both LMF and JSF model (Fig. 8). All participants RWS predictions can be seen in the Supplementary Material.

The default scaled LMF model was not able to follow the experimental volume decrease rate. As payload increased, the LMF model quickly stopped performing on the lateral and frontal far-from-torso RWS regions, corresponding to shoulder abduction and flexion movements, respectively. The top (above-head) portion seemed also to be compromised, especially for simulations using both no-payload and current-payload data.

The JSF model was stronger than the LMF and able to follow the experimental data for heavier payload cases. The most frontal far-from-torso aspect of the predicted RWS was however compromised, which might also relate to shoulder flexion or abduction capabilities.

Lastly, both $V_{sim}$ and $(V_{exp} \cap V_{sim})$ were compared against the original $V_{exp}$ as presented by the Bland-Altman plots in Fig. 9-A/B. Volume-wise, $V_{sim}$ for the LMF and JSF models showed trends of under- and over-estimation, respectively. The accuracy of the volume estimation also decreased with increasing hand-payload, for both models. With respect to $(V_{exp} \cap V_{sim})$, the LMF models

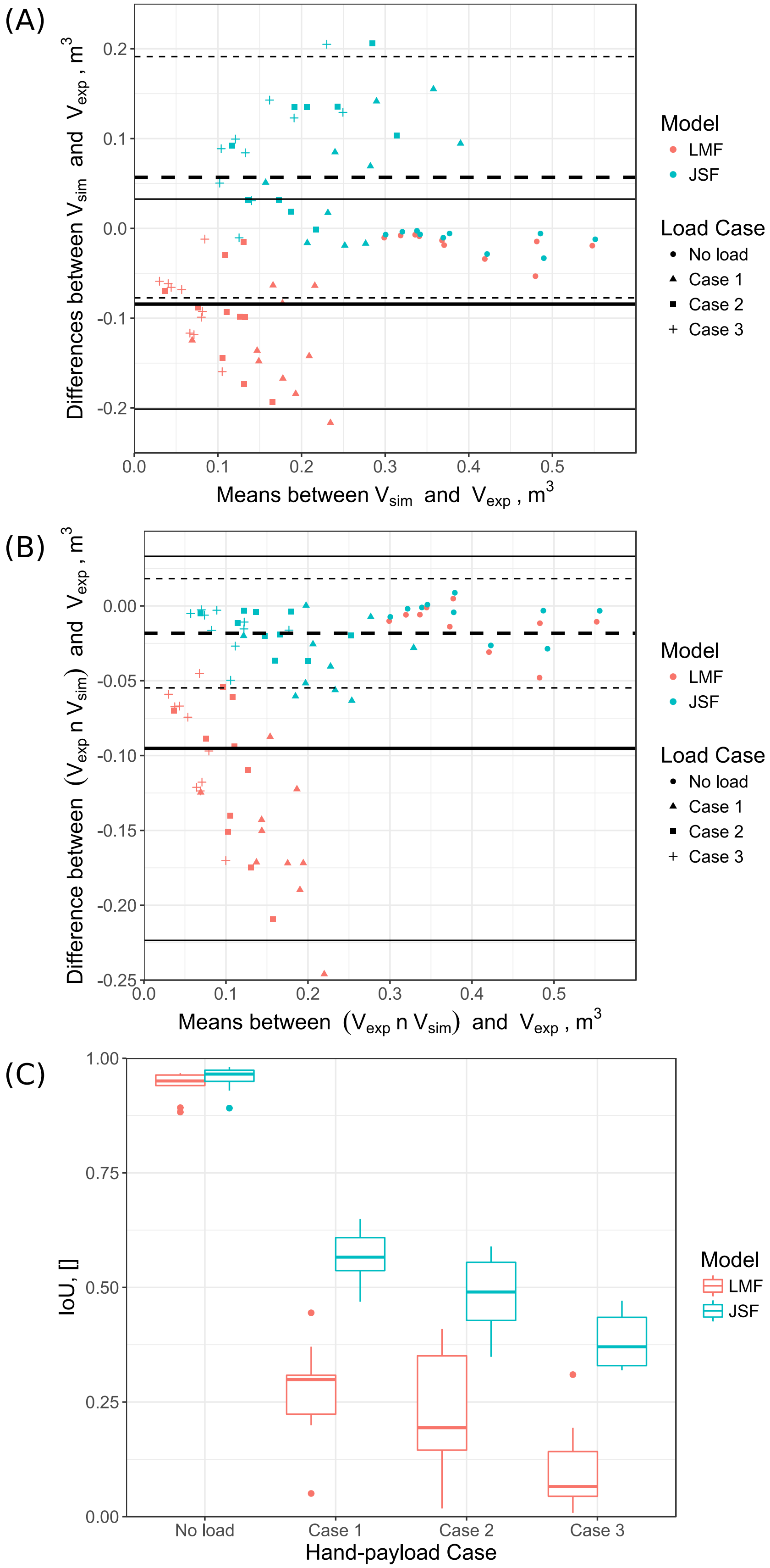

**Fig. 9.** Comparison of the RWS volume predictions for both LMF and JSF models against those measured for the experimental RWS for all payload cases: (A) a Bland-Altman plot between experimental $V_{exp}$ and simulated $V_{sim}$ volumes; (B) a Bland-Altman plot between experimental $V_{exp}$ and intersection $V_{exp} \cap V_{sim}$ volumes; (C) box plots showing the significant Intersection-over-Union (IoU) differences between the LMF and optimized JSF models for all load cases.

behaved poorly while the JSF models nearly estimated the same amount of volume as $V_{exp}$. However, the specific RWS envelope matching between predictions and experimental values were observed using the IoU metric (Fig. 9C), showing that the model performance was the lowest for the LMF models. For all load cases, the differences between IoU values were found to be significant ($p < 0.002$). The JSF models predicted the RWS with more accuracy than did the LMF models.

## 4. Discussion

The results indicate that the subject-specific JSF models perform better than the LMF models. Thus, the use of the RWS as a validation metric captured differences between model predictions. The simulations, as depicted in Fig. 5, showed that the LMF models are generally weak and unable to represent the participants during maximal effort tasks. This finding contradicts the study by Chander and Cavatorta (2018), but this might be explained by the fact that LMF scales relatively to an initial model that is based on cadaver data containing for instance muscle cross sections that are smaller than those for the average person. The use of Hill-type muscle-tendon units with poorly calibrated tendon slack lengths may also influence these results, since they were not further optimised. This variable is known to be the most sensitive (Ackland et al., 2012; Carbone et al., 2016; De Groote et al., 2010; Redl et al., 2007) and can be detrimental to the accuracy given its effect on shifting the force-length curve. A better approximation of the strength measurements was achieved by the JSF models. The optimiser adjusted the isometric strengths through the JSF factors until all MMACTs were as closer to one within the imposed bounds. The higher JSF products revealed for each muscle on Fig. 6 can be explained by the poor performance of the LMF on matching the strength measures of shoulder flexion, abduction, internal and external rotations, and of pushing and pulling tasks. All these reached median values above twice the nominal strength. Nevertheless, such subject-specificity approach can be extended to other upper extremity (Quental et al., 2016; Saul et al., 2015) or lower extremity (Carbone et al., 2015; Rajagopal et al., 2016) models as implemented in other modelling software.

The RWS shape evolution with increasing payload (Fig. 7) showed a shrinkage on both lateral and frontal far-from-torso aspects of the RWS towards an hourglass shape. This can be explained by the larger moments that heavy payloads generate about the shoulder joint for both abduction and flexion movements (Castro et al., 2019). Only close-to-torso regions prevail for heavy payloads. This trend affects all participants as it can be later confirmed by the empirical volume data illustrated in Fig. 9. Both LMF and JSF predictions follow this trend (Fig. 8). However, the muscle-tendon units in the default LMF-scaled model could not reproduce the experimental trend of RWS volume decrease on Fig. 9, most evident for heavier payloads. This suggests that, either by incorrectly estimated muscle isometric strength or poorly calibrated tendon slack lengths, such models are weak. On the other hand, the JSF models performed far better than the LMF scaling, suggesting that subject-specificity is important in musculoskeletal modelling (Hicks et al., 2015; Lund et al., 2012). Nonetheless, since the JSF models could at most present an IoU value of 0.56 for the effective load cases, the lack of accuracy may still relate to the calibrated tendon slack lengths.

This study has some limitations. Even though an effort was made to minimise fatigue, the RWS assessment duration and submaximal isometric contractions cannot be disregarded. Since the participants were not strapped to the chair, it might have contributed for some submaximal contractions that could have influenced our results. On the model side, the computational cost and complexity of optimising also tendon slack lengths was avoided. Preliminary optimisations without the bounds on JSF products resulted in some muscles having products greater than 10, which is not physiological. As the passive muscle stiffness is linked to the isometric muscle strength, this is likely caused by the optimiser overfitting the data using passive forces. To avoid this overfitting, we introduced the bounds but another possible solution could be to include measurements of the arm postures towards the extremes of the ROM but supported such that the subject is fully relaxed. Hereby, terms specifying no or low muscle activities could be added to optimisation problem to ensure that large muscle forces are not necessary at the extreme of the ROM to counteract passive forces. Another important issue regards the accuracy of volume estimation upon very sparse point clouds. This has mostly impact on the heavier payload cases, but such effect is systematic, thus affecting the predictions of both LMF and JSF models.

As a validation metric, the RWS quantified the performance of both models. Still, this metric should be further studied, for instance to establish its sensitivity on the reachable point cloud density while using alpha-shapes. Interpolation with radial basis functions might enable definition of the space with a smaller number of points. Finally, more computational power and perhaps neural networks could investigate the direct sensitivity of both RWS volume and shape to the muscle-tendon unit parameters, thus enabling to scale well-performing and clinically relevant models. Likewise, this validation method can potentially be extended to lower extremity models, since these also behave like open kinematic chains. Consequently, the RWS can be generated and studied for different leg or foot payloads.

## Declaration of Competing Interest

John Rasmussen declares himself as shareholder and CTO of AnyBody Technology A/S. The remaining authors do not have any conflict of interest.

## Acknowledgements

This work was supported by the Danish Strategic Research Council, Denmark and the Danish Council for Technology and Innovation under the Patient@Home (https://www.patientathome.dk/) project. The authors thank to all participants.

## Appendix A. Supplementary data

Supplementary data to this article can be found online at https://doi.org/10.1016/j.jbiomech.2019.04.037.

## References

Ackland, D.C., Lin, Y.-C., Pandy, M.G., 2012. Sensitivity of model predictions of muscle function to changes in moment arms and muscle–tendon properties: a Monte-Carlo analysis. J. Biomech. 45, 1463–1471.

Andersen, M.S., Damsgaard, M., Rasmussen, J., 2009. Kinematic analysis of over-determinate biomechanical systems. Comput. Methods Biomech. Biomed. Engin. 12, 371–384.

Andersen, M.S., Damsgaard, M., MacWilliams, B., Rasmussen, J., 2010. A computationally efficient optimisation-based method for parameter identification of kinematically determinate and over-determinate biomechanical systems. Comput. Methods Biomech. Biomed. Engin. 13, 171–183.

Bolsterlee, B., Vardy, A.N., van der Helm, F.C.T., (DirkJan) Veeger, H.E.J., 2015. The effect of scaling physiological cross-sectional area on musculoskeletal model predictions. J. Biomech. 48, 1760–1768.

Box, M.J., 1965. A new method of constrained optimization and a comparison with other methods. Comput. J. 8, 42–52.

Box, G.E., Behnken, D.W., 1960. Some new three level designs for the study of quantitative variables. Technometrics 2, 455–475.

Carbone, V., Fluit, R., Pellikaan, P., van der Krogt, M.M., Janssen, D., Damsgaard, M., Vigneron, L., Feilkas, T., Koopman, H.F.J.M., Verdonschot, N., 2015. TLEM 2.0 – a comprehensive musculoskeletal geometry dataset for subject-specific modeling of lower extremity. J. Biomech. 48, 734–741.

Carbone, V., van der Krogt, M.M., Koopman, H.F.J.M., Verdonschot, N., 2016. Sensitivity of subject-specific models to Hill muscle-tendon model parameters in simulations of gait. J. Biomech. 49, 1953–1960.

Castro, M.N., Rasmussen, J., Bai, S., Andersen, M.S., 2019. The reachable 3-D workspace volume is a measure of payload and body-mass-index: a quasi-static kinetic assessment. Appl. Ergon. 75, 108–119.

Chander, D.S., Cavatorta, M.P., 2018. Multi-directional one-handed strength assessments using anybody modeling systems. Appl. Ergon. 67, 225–236.

Damsgaard, M., Rasmussen, J., Christensen, S.T., Surma, E., de Zee, M., 2006. Analysis of musculoskeletal systems in the anybody modeling system. Simul. Model. Pract. Theory 14, 1100–1111.

De Groote, F., Van Campen, A., Jonkers, I., De Schutter, J., 2010. Sensitivity of dynamic simulations of gait and dynamometer experiments to hill muscle model parameters of knee flexors and extensors. J. Biomech. 43, 1876–1883.

de Zee, M., Hansen, L., Wong, C., Rasmussen, J., Simonsen, E.B., 2007. A generic detailed rigid-body lumbar spine model. J. Biomech. 40, 1219–1227.

Edelsbrunner, H., Mücke, E., 1994. Three-dimensional alpha shapes. ACM Trans. Graph. 13, 43–72.

Fischer, M.C.M., Eschweiler, J., Schick, F., Asseln, M., Damm, P., Radermacher, K., 2018. Patient-specific musculoskeletal modeling of the hip joint for preoperative planning of total hip arthroplasty: a validation study based on in vivo measurements. PLoS One 13, 1–19.

Fleming, B.C., Beynnon, B.D., 2004. In vivo measurement of ligament/tendon strains and forces: a review. Ann. Biomed. Eng. 32, 318–328.

Fluit, R., Andersen, M.S., Kolk, S., Verdonschot, N., Koopman, H.F.J.M., 2014. Prediction of ground reaction forces and moments during various activities of daily living. J. Biomech. 47, 2321–2329.

Frankenfield, D.C., Rowe, W.A., Cooney, R.N., Smith, J.S., Becker, D., 2001. Limits of body mass index to detect obesity and predict body composition. Nutrition 17, 26–30.

Fregly, B.J., Boninger, M.L., Reinkensmeyer, D.J., 2012. Personalized neuromusculoskeletal modeling to improve treatment of mobility impairments: a perspective from European research sites. J. Neuroeng. Rehabil. 9, 1–11.

Garner, B.A., Pandy, M.G., 2003. Estimation of musculotendon properties in the human upper limb. Ann. Biomed. Eng. 31, 207–220.

Han, J.J., de Bie, E., Nicorici, A., Abresch, R.T., Bajcsy, R., Kurillo, G., 2015. Reachable workspace reflects dynamometer-measured upper extremity strength in FSHD. Muscle Nerve 2, 1–8.

Heinen, F., Lund, M.E., Rasmussen, J., de Zee, M., 2016. Muscle-tendon unit scaling methods of Hill-type musculoskeletal models: An overview. Proc. Inst. Mech. Eng. Part H J. Eng. Med. 230, 976–984.

Hicks, J.L., Uchida, T.K., Seth, A., Rajagopal, A., Delp, S., 2015. Is my model good enough? best practices for verification and validation of musculoskeletal models and simulations of human movement. J. Biomech. Eng. 137, 020905.

Klopčar, N., Tomšič, M., Lenarčič, J., 2007. A kinematic model of the shoulder complex to evaluate the arm-reachable workspace. J. Biomech. 40, 86–91.

Lee, H., Jung, M., Lee, K.-K., Lee, S., 2017. A 3D human-machine integrated design and analysis framework for squat exercises with a smith machine. Sensors 17, 299.

Lloyd, D.G., Besier, T.F., 2003. An EMG-driven musculoskeletal model to estimate muscle forces and knee joint moments in vivo. J. Biomech. 36, 765–776.

Lund, M.E., Zee, M. De, Andersen, M.S., de Zee, M., Andersen, M.S., Rasmussen, J., 2012. On validation of multibody musculoskeletal models. Proc. Inst Mech. Eng. Part H J. Eng. Med. 226, 82–94.

Marra, M.a., Vanheule, V., Fluit, R., Koopman, B.H.F.J.M., Rasmussen, J., Verdonschot, N., Andersen, M.S., 2015. A subject-specific musculoskeletal modeling framework to predict in vivo mechanics of total knee arthroplasty. J. Biomech. Eng. 137, 020904.

Matthew, R.P., Kurillo, G., Han, J.J., Bajcsy, R., 2015. Calculating Reachable Workspace Volume for Use in Quantitative Medicine. In: Agapito, L., Bronstein, M.M., Rother, C. (Eds.), ECCV 2014 Workshops, Part III, Lecture Notes in Computer Science. Springer International Publishing, Cham, pp. 570–583.

Moore, K.L., Agur, A.M., 2007. Essential Clinical Anatomy, 3rd. Lippincott Williams & Wilkins, Baltimore, USA.

Pontonnier, C., de Zee, M., Samani, A., Dumont, G., Madeleine, P., 2014. Strengths and limitations of a musculoskeletal model for an analysis of simulated meat cutting tasks. Appl. Ergon. 45, 592–600.

Quental, C., Folgado, J., Ambrósio, J., Monteiro, J., 2013. Multibody system of the upper limb including a reverse shoulder prosthesis. J. Biomech. Eng. 135, 111005.

Quental, C., Folgado, J., Ambrósio, J., Monteiro, J., 2016. A new shoulder model with a biologically inspired glenohumeral joint. Med. Eng. Phys. 38, 969–977.

Rajagopal, A., Dembia, C.L., DeMers, M.S., Delp, D.D., Hicks, J.L., Delp, S.L., 2016. Full-body musculoskeletal model for muscle-driven simulation of human gait. IEEE Trans. Biomed. Eng. 63, 2068–2079.

Rasmussen, J., Damsgaard, M., Voigt, M., 2001. Muscle recruitment by the min/max criterion — a comparative numerical study. J. Biomech. 34, 409–415.

Rasmussen, J., Zee, M De, Damsgaard, M., Christensen, S.T., Marek, C., Siebertz, K., 2005. A General Method for Scaling Musculo-Skeletal Models. In: International Symposium on Computer Simulation in Biomechanics. Cleveland, OH, USA, p. 70220914.

Rasmussen, J., Holmberg, L.J., Sørensen, K., Kwan, M., Andersen, M.S., de Zee, M., 2012. Performance optimization by musculoskeletal simulation. Mov. Sport Sci. – Sci. Mot. 83, 73–83.

Redl, C., Gfoehler, M., Pandy, M.G., 2007. Sensitivity of muscle force estimates to variations in muscle-tendon properties. Hum. Mov. Sci. 26, 306–319.

Sartori, M., Llyod, D.G., Farina, D., 2016. Neural data-driven musculoskeletal modeling for personalized neurorehabilitation technologies. IEEE Trans. Biomed. Eng. 63, 879–893.

Saul, K.R., Hu, X., Goehler, C.M., Vidt, M.E., Daly, M., Velisar, A., Murray, W.M., 2015. Benchmarking of dynamic simulation predictions in two software platforms using an upper limb musculoskeletal model. Comput. Methods Biomech. Biomed. Engin. 18, 1445–1458.

Valente, G., Pitto, L., Testi, D., Seth, A., Delp, S.L., Stagni, R., Viceconti, M., Taddei, F., 2014. Are subject-specific musculoskeletal models robust to the uncertainties in parameter identification? PLoS One 9, e112625.

Van der Helm, F.C.T., Veeger, H.E.J., Pronk, G.M., Van der Woude, L.H.V., Rozendal, R. H., 1992. Geometry parameters for musculoskeletal modelling of the shoulder system. J. Biomech. 25, 129–144.

Veeger, H.E.J., Van Der Helm, F.C.T., Van Der Woude, L.H.V., Pronk, G.M., Rozendal, R. H., 1991. Inertia and muscle contraction parameters for musculoskeletal modelling of the shoulder mechanism. J. Biomech. 24, 615–629.

Veeger, H.E.J., Yu, B., An, K.-N., Rozendal, R.H., 1997. Parameters for modeling the upper extremity. J. Biomech. 30, 647–652.

Wu, J.Z., Chiou, S.S., Pan, C.S., 2009. Analysis of musculoskeletal loadings in lower limbs during stilts walking in occupational activity. Ann. Biomed. Eng. 37, 1177–1189.

Zajac, F.E., 1989. Muscle and tendon: properties, models, scaling, and application to biomechanics and motor control. Crit. Rev. Biomed. Eng. 17, 359–411.